Regular Article

Very long-range attractive and repulsive forces in model colloidal dispersions

Alfredo González-Calderón[1,a], Enrique González-Tovar[2],
and Marcelo Lozada-Cassou[1,b]

[1] Instituto de Energías Renovables, Universidad Nacional Autónoma de México
(U.N.A.M.), 62580 Temixco, Mor., Mexico
[2] Instituto de Física, Universidad Autónoma de San Luis Potosí, Álvaro Obregón 64,
78000 San Luis Potosí, S.L.P., Mexico

Abstract. Experiments with polymer latex solutions show the coexistence of order-disorder structures of macroions. Because of the large macroions' sizes, this order–disorder phase coexistence imply the existence of very long-range attractive and repulsive forces, which cannot be explained in terms of conventional direct interaction potentials, which are short-range. Here, we apply an integral equations theory to a simple model for colloidal dispersions, at finite concentrations, calculate the particles distribution functions and the involved effective forces. We find very long-range attractive and repulsive forces among the like-charged macroions. The distribution functions are in qualitative agreement with experimental results. The origin of these forces are discussed in terms of an energy–entropy balance.

1 Introduction

The study of the interactions of charged colloidal particles or macromolecules is relevant in the fields of physics, chemistry, biology, energy and technology [1–4]. In particular, suspensions of highly charged colloidal particles or macromolecules, depending on the volume fractions, salt concentrations, and temperature, can form gas, liquid and crystal structures [5–7], and order–disorder coexistence regions [8–11]. Because of the large macroions' sizes, this experimentally found order–disorder phases coexistence implies the existence of very long-range repulsive and attractive forces, which cannot be explained in terms of conventional direct interaction potentials, which are of relatively short range [12]. Particularly puzzling is the existence of a long-range attraction among like-charged particles. To explain this long-range attraction, semi-phenomenological long-range potentials were proposed [13–15]. Both, the theoretical approach and the experimental results have been questioned by different authors [16–19], either arguing the semi-phenological nature of the proposed potential and/or that the experimentally observed order–disorder coexistence

---

[a] *Present address*: CONACyT - Centro de Ingeniería y Desarrollo Industrial (CIDESI), Av. Playa Pie de la Cuesta 702, Desarrollo San Pablo, 76125 Querétaro, Qro., Mexico.
[b] e-mail: marcelolcmx@ier.unam.mx

was a result of the system not being in equilibrium and/or being in confinement. However, the criticisms to the experimental results seem to have been properly responded [11,20–22]. Hence, the main experimental finding, i.e., *there is a long-range attraction between like-charged particles, at finite colloids concentration*, is probably correct. But, then, does this attractive force exist, and if it does exist what is the origin of this long-range attraction? Ise et al. [13,23,24] have proposed that this attraction is due to "*an intermacroion attraction through the intermediary of counterions balanced by intermacroion repulsion*". While in this article we do not try to find an order–disorder coexistence curve, we do address the above questions, and calculate the macroion–macroion forces, through a well-established liquid theory. We do, indeed, find a long-range attraction force. We hope to help to clarify this controversy, and offer a mechanism to explain this attraction. In this paper, we extend our previous calculations for macroions dispersions, at finite concentrations [25], where we studied the effect of the location of the macroions charge, and reported a long-range macroion–macroion correlation. Here, we provide new results for macroions forces, give a detailed analysis of their foundations, nature, and range, offer an explanation for our reported long-range attractive-repulsive forces, and exhibit a comparison with existing experimental data. In Section 2, we present our theoretical approach. In Section 2.1, we outline the derivation of the integral equations. In Section 2.2, we describe the model for a macroions solution, at finite volume fraction, and outline the formulation of the electrostatics and forces in the system. In Section 3, we report the results for the radial distribution functions (RDFs), the electrical field, and the mean forces among the like-charged macroions. Finally, in Section 4 we give some conclusions.

2 Theory

Most studies on charged colloidal suspensions are made for isolated macroions or two like-charged colloids particles, i.e., at infinite dilution, immersed into a model electrolyte [26–33]. Theoretical and simulation investigations of nano-particles suspensions at finite volume fractions are technically more difficult due to the large increase of integration space (with different length scales) in theoretical equations, or the huge number of particles in, necessarily, larger simulation boxes. Thus, many studies used some kind of charge renormalization [34–37], colloidal suspensions with no salt added [38], or very low salt concentration [18]. In general, these investigations are for relatively low colloidal charge and volume fraction [39,40].

Since the pioneer development of the integral equations by Kirkwood et al. [27,41], for homogeneous and inhomogeneous size-symmetrical electrolytes, based on a density expansion plus a superposition approximation, other approximated integral equations based on the Ornstein–Zernike (OZ) equation [42] have been derived. Among them is the hypernetted-chain/mean spherical approximation (HNC/MSA) [43,44], first proposed by Carnie et al. in 1981 [45]. In this report, we solve these integral equations for a model of three species electrolyte solution. In this section, we outline the derivation of the HNC/MSA equation, with which we will obtain the RDFs of the macroions solution, describe the macroions' model, and give the expressions of the relevant electrostatic variables and interparticle's mean forces, in terms of the RDFs.

2.1 The hypernetted-chain/mean spherical equations

In our model, the particles are taken to be charged, hard spheres, with different charges and diameters, such that one of the species is much larger than the other two, in order to model a macroions dispersion at finite concentration. We will refer

to his model as the colloidal primitive model (CPM) [25,46,47], which is a variant of the well-known primitive model [48,49].

The multicomponent OZ equation for a fluid of n species is given by $h_{ij}(\mathbf{r}_{21}) = c_{ij}(\mathbf{r}_{21}) + \sum_{l=1}^{n} \rho_l \int_V h_{il}(\mathbf{r}_{23})c_{lj}(\mathbf{r}_{31})d\mathbf{r}_3$, where V is the system's volume, $i,j = 1, 2, \ldots, n$, and ρ_l is the number density of species l. $h_{ij}(\mathbf{r}_{21}) \equiv g_{ij}(\mathbf{r}_{21}) - 1$ is the total correlation functions for two particles at $\mathbf{r}_2$ and $\mathbf{r}_1$, of species i and j, respectively, with $\mathbf{r}_{21} = \mathbf{r}_2 - \mathbf{r}_1$, such that $g_{ij}(\mathbf{r}_{21})$ is the pair correlation function, also referred to as the RDF, which gives the probability density of finding a particle 1, of species j, at the distance $\mathbf{r}_{21}$, from the central particle 2, of species i. The OZ equation is a probability balance, that guaranties a constant chemical potential in the whole system [50]. To solve it, closure relations for the direct correlation functions, $c_{ij}(\mathbf{r}_{21})$ and $c_{lj}(\mathbf{r}_{31})$, are needed. These functions are basically approximations for a quasi-particle, in the context of many-body theory [51]. Among others, two direct correlation approximations have been successfully used, the hypernetted-chain (HNC), defined as $c_{ij}(\mathbf{r}_{21}) = -\beta u_{ij}(\mathbf{r}_{21}) + h_{ij}(\mathbf{r}_{21}) - \ln g_{ij}(\mathbf{r}_{21})$, and the Mean Spherical (MSA) as $c_{il}(\mathbf{r}_{21}) = -\beta u_{ij}(\mathbf{r}_{21})$, where $\beta = 1/(kT)$, k is the Boltzmann constant, T is the system temperature, and $u_{ij}(\mathbf{r}_{21})$ is the, unscreened, pair-interaction potential between particles 1 and 2. If the HNC approximation is used in the first term of the right-hand side of the OZ equation, we obtain

$$g_{ij}(\mathbf{r}_{21}) = \exp\left\{-\beta u_{ij}(\mathbf{r}_{21}) + \sum_{l=1}^{n} \rho_l \int_V h_{il}(\mathbf{r}_{23})c_{lj}(\mathbf{r}_{31})d\mathbf{r}_3\right\}. \tag{1}$$

If $c_{lj}(\mathbf{r}_{31})$, inside the integral in equation (1), is taken to be given by the MSA, for which there is an analytical solution for charged fluids [52], we get the HNC/MSA integral equations, for an homogeneous fluid of n-species. The use of the MSA allows to have analytical kernels in equation (1). A detail account of the derivation of equation (1) for the CPM is given in Manzanilla-Granados et al. [25].

2.2 The model, radial distribution functions, electrostatics, and forces

For a system of three species fluid, equation (1) becomes a set of six, coupled, non-linear integral equations, which as we are taking advantage of the analytical solution for the MSA can be reduced to three coupled integral equations. We numerically solve these equations with a finite elements method developed in the past for the solution of integral equations [25,53,54].

We solve equation (1) for the CPM, for a three species charged fluid, i.e., positive ions, negative ions, and macroions of species $+$, $-$, and M, respectively. For simplicity, we will assume the macroions to be positive large particles of diameter a_M, and all the little ions of equal size, including the macroions' counterions (the case in which the macroions are negatively charged is symmetrical to the positively charged macroions case). Thus, the ions's diameters are $a_+ = a_- \equiv a$. Therefore, from the solution of equation (1) we obtain the macroion–macroion, $g_{MM}(r)$, macroion–anion, $g_{M-}(r)$, and macroion–cation, $g_{M+}(r)$, RDFs. The other three distribution functions, i.e. $g_{--}(r)$, $g_{++}(r)$, and $g_{+-}(r)$, are analytically obtained from the MSA [52].

The interaction potential between two particles of species i and j, with a separation distance r, is given by

$$u_{ij}(r) = \begin{cases} \infty & \text{for } r < a_{ij} \\ \dfrac{e^2 z_i z_j}{\epsilon r} & \text{for } r \geq a_{ij} \end{cases} \quad \text{with } i,j = +, -, M \tag{2}$$

where $a_{ij} = (a_i + a_j)/2$, e is the proton charge, z_i and z_j are the valences of particles of species i and j, respectively, and ϵ is the solvent dielectric constant, and such that the system is electroneutral ($\sum_{j=+,-,M} ez_j \rho_j = 0$). Both the electrolyte ions and macroions are assumed to have the same dielectric constant as that of the solvent, to avoid image charges. For a colloid's valence Z_M, its surface charge density is $\sigma_M = Z_M e/(\pi a_M^2)$. Hence, its unscreened charge is $Q_M = \pi a_M^2 \sigma_M$. However, in general, the colloid's effective charge, at a distance r from its center (i.e., its bare charge Q_M, plus the induced charge in the surrounding fluid, up to a distance r), is given by

$$Q_M(r) = Q_M + 4\pi \int_{a_M/2}^{r} \rho_{el}(t) t^2 dt = -4\pi \int_{r}^{\infty} \rho_{el}(t) t^2 dt \tag{3}$$

where

$$\rho_{el}(r) \equiv \sum_{j=+,-,M} ez_j \rho_j g_{Mj}(r) \tag{4}$$

is the charge concentration profile around the central colloidal particle, and we have used the electroneutrality condition for the bulk fluid, given by

$$Q_M = -4\pi \int_{a_M/2}^{\infty} \rho_{el}(t) t^2 dt. \tag{5}$$

Equation (3) implies that as $r \to \infty$, $Q_M(r) \to 0$. While Q_M and $Q_M(r)$ give the macroions bare charge, and effective charge at every distance r from the center of the reference macroion, the surface charge density is often used in the literature to report colloids' experimental and theoretical studies. Hence, we define the charge density profile, $\sigma_M(r)$, around the central macroion, as

$$\sigma_M(r) \equiv \sigma_M \frac{R_M^2}{r^2} + \frac{1}{r^2} \int_{R_M}^{r} \rho_{el}(t) t^2 dt, \tag{6}$$

where $R_M = a_M/2$ is the macroion radius, σ_M is its surface charge density, and the second term in equation (6) is the induced charge in the fluid around the central particle from R_M to r. In terms of σ_M, equation (5) can be written as

$$\sigma_M = -\frac{1}{R_M^2} \int_{R_M}^{\infty} \rho_{el}(t) t^2 dt. \tag{7}$$

Hence, equation (6) can also be expressed as

$$\sigma_M(r) = -\frac{1}{r^2} \int_{r}^{\infty} \rho_{el}(t) t^2 dt. \tag{8}$$

By Gauss' law, the electrical field, $E_M(r)$, at the distance r from the center of the reference particle, is $E_M(r) = 4\pi \sigma_M(r)/\epsilon$.

On the other hand, equation (1) can be recast as [25]

$$g_{ij}(\mathbf{r}_{21}) = \exp\left\{ -\beta q_j \psi_{ij}(\mathbf{r}_{21}) + \beta \omega_{ij}^{sr}(\mathbf{r}_{21}) \right\}, \tag{9}$$

where $\psi_{ij}(\mathbf{r}_{21})$ is the mean electrostatic potential, given by

$$\psi(r) = \frac{4\pi}{\epsilon} \int_r^\infty \rho_{el}(t) \left(t - \frac{t^2}{r} \right) dt, \tag{10}$$

and $\omega_{ij}^{sr}(\mathbf{r}_{21})$ is a mean potential of the short-range force. Thus, the potential of mean force, given by

$$W_{ij}(\mathbf{r}_{21}) \equiv -kT \ln g_{ij}(r) = ez_j \psi_{ij}(\mathbf{r}_{21}) + \omega_{ij}^{sr}(\mathbf{r}_{21}), \tag{11}$$

contains the contributions from the electrostatic and short-range correlations, between the central particle of species i and another particle in the fluid of species j. Therefore, the total mean force is equal to the sum of the electrostatic and short-range components, i.e.,

$$F_{ij}^T(r) = F_{ij}^e(r) + F_{ij}^s(r), \tag{12}$$

with $F_{ij}^T(r) = -d(W_{ij}(r))/dr$, $F_{ij}^e = -ez_j d(\psi_{ij}(r))/dr = ez_j E_M(r)$ and $F_{ij}^s = -d(\omega_{ij}^{sr}(r))/dr$, respectively, where we have taken advantage of the spherical symmetry of the system, and have omitted the subindexes for simplicity. Here, we will refer to the short-range component of the force as the entropic component.

Although the mean force is equal to the sum of the entropic and electrostatic force components, these two components are entangled or intertwined, through the non-linear integral equation (9), *since both components (electrostatic and entropic) are dependent functionals of the RDF,* $g_{ij}(r)$. *The entanglement of the entropy and energy contributions to the total system energy is beyond the non-linearity of equation* (9), *as can be seen from equation* (11), *i.e., a change in* Q_M, ρ_i *and* a_i, *for any of the ionic species,* ϵ *and/or* T *will modify simultaneously* $\psi_{ij}(\mathbf{r}_{21})$ *and* $\omega_{ij}^{sr}(\mathbf{r}_{21})$. *This entanglement of the electrical and entropic components of the fluid energy should not be confused with its use in quantum mechanics or mathematical psychology, among other science fields* [55].

The total force between the central macroion, of species M, and an ion of species i, $F_{Mi}^T(r)$, was calculated by numerical derivation of the potential of mean force, i.e., $F_{Mi}^T(r) = -dW_{Mi}(r)/dr = kT dln[g_{Mi}(r)]/dr$. Its electrostatic component, $F_{Mi}^e(r)$, was calculated by numerical derivation of equation (10) and/or directly from $eZ_M E_M(r) = 4\pi e Z_M \sigma_M(r)/\epsilon$, with the aid of equation (8). Its entropic component, $F_{Mi}^s(r)$, was calculated from the difference of the total and electrical forces, and/or through the contact values of the different RDFs, $g_{Mi}(r = a_{Mi}/2)$, i.e., with $F_{Mi}^s(r) = \sum_{j=+,-,M} \rho_j g_{Mj}(r; a_{Mj}/2)$. The contact values, of course, are different for different values of the position r of the particle of species i. *All the different procedures for the calculations of the total force components were found to be consistent.*

3 Results

With the RDFs obtained from equation (1) we calculate the total force, and its electric and entropic components, for macroions at several colloidal volume fractions, $\phi \equiv \frac{1}{6}\pi\rho_M a_M^3$, and surface charge densities σ_M, i.e., several macroions' valences, Z_M. In all cases, unless otherwise indicated, the added salt is a 1:1, 0.1 M electrolyte, with ionic diameter, $a = 4.25\,\text{Å}$, and the macroions' diameter is $a_M = 10a$. The solvent dielectric constant is taken to be $\epsilon = 78.5$, and the system temperature $T = 298\,\text{K}$.
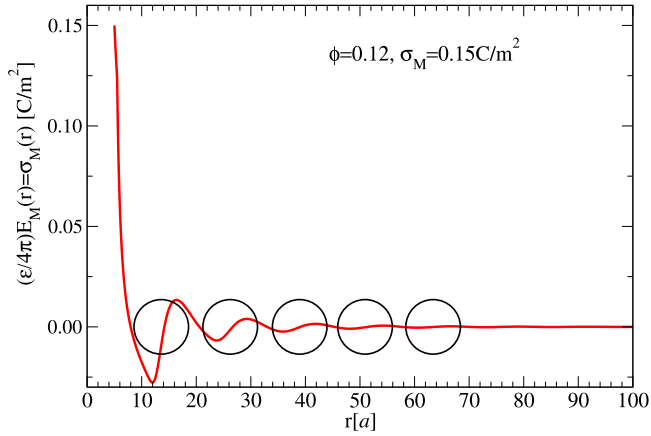
Fig. 1. Electrical field and charge density profiles, around the reference macroion, measured from its center. The circles positions, in r, coincide with the maxima in the radial distribution function. $\rho_{\text{salt}} = 0.1\text{M}$, $a_M = 10a$.

### 3.1 Long-range attractive and repulsive forces: detailed analysis and charge dependence

In Figure 1, we present the HNC/MSA results for the macroion's charge density profile, $\sigma_M(r) = (\epsilon/4\pi)E_M(r)$, as a function of the distance, r, to the center of the central particle, for $\phi = 0.12$, and surface charge density, $\sigma_M = 0.15\,\text{C/m}^2(Z_M \approx 53)$, thus (of course), from equation (8), $\sigma_M(r = 5a) = 0.15\,\text{C/m}^2$, on the surface of the central, reference particle. As was pointed out above, the $\lim_{r\to\infty} \sigma_M(r) \to 0$, to satisfy the electroneutrality of the bulk fluid, and was numerically corroborated in our calculations.

A number of sequential charge inversions is observed, indicating the change of direction of the electrical field, $E_M(r)$. The locations of the maxima and minima of the charge density in the fluid are closely related to the macroions' size, volume fraction, surface charge and location, and show interesting new surface phenomena [56,57]. However, in this article we address only to the foundations, nature and range of the forces among charged macroions.

The dimension and location of the circles shown in Figure 1 correspond exactly to the size and most probable location of the layers of neighboring macroions, around the reference macroion, according to the corresponding RDF (see Tab. 1). Their location does not coincide with the inflection points of the charge profile curves, since these are the points of zero electrical field, but not of zero force. We will come back to this point later. Notice that the charge inversions occur before (negative) and after (positive) the position of the positively charged macroions, indicating the effect of the adsorbed negative ions. Because the negative ions are the sum of the salt anions plus the macroions' counterions, the molar concentration of the anions, for a macroions dispersion with $\phi = 0.12$, and $\sigma_M = 0.15\,\text{C/m}^2$, is $\rho_- = 0.3634M$, which is more than three times that of the little cations ($\rho_+ = 0.1M$). From $r = 5a$, i.e., from the surface of the central macroion, up to $r \approx 12a$ the charge density is seen to rapidly decrease down to $\sigma_M(r = 11.88a) \approx -0.028\,\text{C/m}^2$. The position of this first correlated macroions' layer is $r \approx 13.59a = 1.359a_M$. Then the charge density profile increases up to $\sigma \approx 0.0135\,\text{C/m}^2$, at $r = 16.5a$. This qualitative behavior of the charge density profile continues up to around $250a$. The $\lim_{r\to\infty} \sigma_M(r) \to 0^-$, which implies that the net electrical field is, overall, cohesive, but counterbalanced

Table 1. Location of the first six maxima in the corresponding RDFs, given in units of [a], measured from the center of the reference, central macroion, for six different macroions charge densities, and at a fixed volume fraction, $\phi = 0.12$. Notice that because $a_M = 10a$, by dividing by 10, all the distances reported in this table straightforwardly can be expressed in terms of a_M, a unit of measure used in several experimental reports of the structure of polystyrene latex particles.

| $\sigma_M(\text{C/m}^2)$	First	Second	Third	Fourth	Fifth	Sixth
0.000	10.00	24.22	36.45	48.43	–	–
0.005	10.00	24.47	36.95	48.93	–	–
0.025	13.59	28.22	42.44	56.91	70.80	–
0.050	14.14	28.47	42.44	56.42	70.39	84.87
0.150	13.59	26.22	38.95	50.93	63.40	75.88
0.300	12.47	24.72	36.45	47.93	59.41	70.89
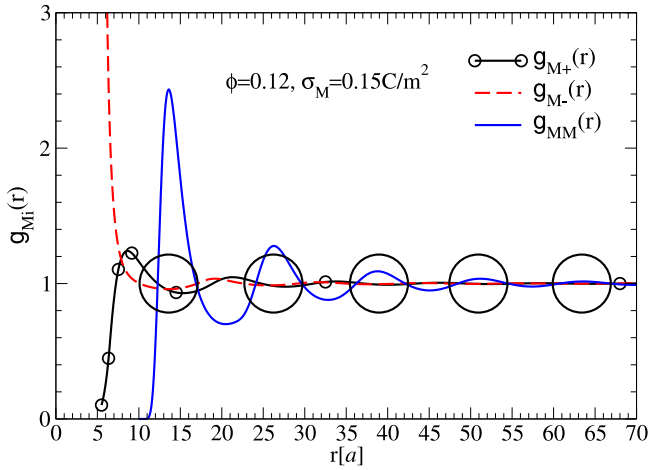
Fig. 2. Radial distribution function, around the central macroion, measured from its center. The circles have the same meaning as in Figure 1. $\rho_{\text{salt}} = 0.1$M, $a_M = 10a$.

by the entropic repulsion. In Table 1, the distance to the central macroion of this first correlated macroions' layer increases, for very low surface charge densities, and decreases for low to high surface charge densities. We will come back to this point later in this article.

In Figure 2, we show RDFs for the macroions, $g_{MM}(r)$, little cations, $g_{M+}(r)$, and anions, $g_{M-}(r)$, as a function of the distance r, to the center of the reference macroion, and for the same solution parameters, as in Figure 1. The anions are strongly adsorbed to the central macroion, while the cations and macroions are repelled to some distance away, i.e., their RDFs are below their bulk values ($g_{MM}(r)$ and $g_{M+}(r)$ are below 1). The RDFs are oscillatory, with the first six maxima of $g_{MM}(r)$ located at $r/a \approx 13.59, 26.22, 38.95, 50.93, 63.40, 75.88$ (see Tab. 1). Hence, the wavelength of the oscillation of the macroions layers is first $\lambda \approx 13.59a$, and later $\lambda \approx 12.5a$. Between the second ($r \approx 13.59a$) and third ($r = 26.22a$) layers of macroions, the anions and cations are seen to oscillate around their bulk values, but with a relatively high adsorption of anions next to the first layer of macroions, at $r \approx 13.59a$, and cations to the second layer of macroions, at $r \approx 26.22a$.

Therefore, intermediated to two neighboring layers of macroions can be fitted between 2 and 3.5 layers of ions. This behavior is repeated for the rest of the macroions layers. From $r \approx 19a$ to $r \approx 22a$, *both, $g_{M-}(r)$ and $g_{M+}(r)$ are simultaneously above*
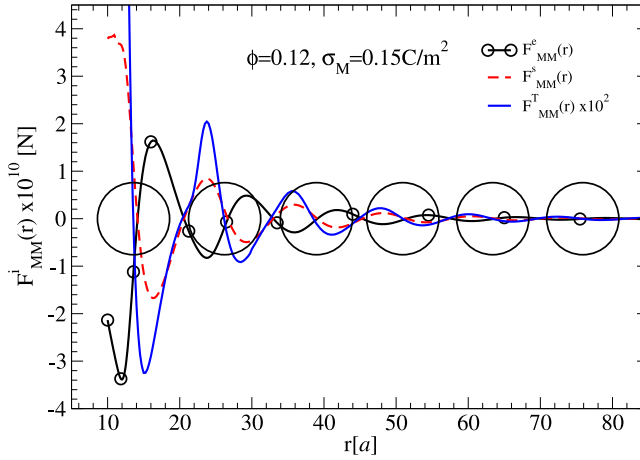
Fig. 3. Mean force among like-charged macroions, and its electrical and entropic components, as a function of the distance to the center of the reference macroion. The circles have the same meaning as in Figure 1. $\rho_{\text{salt}} = 0.1\,\text{M}$, $a_M = 10a$.

their bulk values. This is a very unusual behavior. This effect is not observed in bulk electrolytes [58], electrolytes next to a charged electrode [59–61], confined electrolytes [62] or macroions [63,64]. An exception was reported for the interface of a cylindrical electrode, with surface charge of $0.1544\,\text{C/m}^2$, and a symmetrical 1:1 electrolyte, with a relatively large ionic diameter of 7.4 Å [60], showing the relevance of the ions excluded volume. However, a previous comparison of this theory with molecular dynamics calculation shows a very good qualitative and quantitative agreement in this feature effect [47], and clearly is a consequence of the finite concentration of the large colloidal particles, i.e., excluded volume effect.

Whence, the structure around the central macroion seems to be a sequence of layers macroion–anion–cation–macroion. However, as pointed out before, for these conditions of ϕ and σ_M, $\rho_- = 3.63\rho_+$, and thence the number of anions greatly overcomes the number of cations, around the macroions. This suggests that the macroion–macroion attraction is, at least, partially due to the anions adsorption.

In Figure 3, the total mean force, $F_{MM}^T(r)$, and its electric, $F_{MM}^e(r)$, and entropic, $F_{MM}^s(r)$, components, among the positively charged macroions, are plotted as a function of the distance r from the central macroion. The solution parameters are the same as in Figure 1. Counterintuitively the electric force is attractive, while the entropic force is repulsive, before the first layer of macroions, located at $r \approx 13.59$, to become both, later, oscillatory. A comparison of Figures 1–3 suggests that the first electric attraction is due to the anions adsorbed to the macroions, and the later repulsive electric force is due to the charge of the first layer of macroions. On the other hand, the little negative and positive ions present before the first layer of macroions produces the entropic repulsive force, as an excluded volume effect. The entropic force always overcomes the electric component. Notice that $F_{MM}^T(r)$ is two orders of magnitude lower than its components, so in Figure 3 we have rescaled $F_{MM}^T(r)$. We have drawn six circles, which have the same size as the macroions, and their locations were obtained from the corresponding RDF (see Fig. 2 and Tab. 1). The position of the circles correspond to the six first induced layers of macroions, around the central macroion. *Their centers coincide with the points of zero total force*, as they should have, which, on the other hand, corroborates the correctness of our forces calculations.

Let us see this in some more detail. The first minimum of the electrostatic force occurs at $r \approx 12a$, which corresponds to a distance around $R_M + 7a$, from

the center of the reference macroion. The reduced concentration profile of anions, i.e., $g_{M-}(r)$ (see Fig. 2), shows a very high adsorption of negative charge, from $r = 5.5a$ down to its bulk value, $g_{M-}(r = 10.083a) \lesssim 1.0$, thus overscreening the central macroion charge. At $r = 10a$ we see $F_{MM}^e(r)$ to begin its attractive behavior, and then increasing the attraction intensity up to $r = 12a$, to then decreasing the attraction until $r \approx 14.1205a$, where $F_{MM}^e = 0$. The minimum of the anions RDF is $g_{M-}^{\mathrm{minimum}}(r = 13.5a) = 0.958615$. As a result, we see in Figure 1, the electrical field going from positive values, at $r = 5a$, due to the central macroion charge, down to zero, at $r \approx 7.97a$, then to a minimum, at $r = 12a$, where the cations RDF ($g_{M+}(r)$) goes from its maximum, at $r \approx 8.625$, to its bulk value, at $r \approx 12.25a$. Then $E_M(r)$ increases up to zero, at $r \approx 14.16a$, and then to a maximum, at $r \approx 16.25a$, now due to the first layer of macroions charge, located at $r \approx 13.5935a$. The first maximum of the entropic force occurs at $r \approx 10.92a$, which seems to correspond to a maximum of adsorbed anions plus cations, from $r = 5.5a$ to $r \approx 11a$, i.e., in Figure 2 we see a strong adsorption of anions, much above its bulk value, from $r = 5.5a$, the central-macroion-anion contact value, up to $r \approx 10.08$, where they reach their bulk value (i.e., where $g_{M-}(r = 10.08a) \approx 1$), then down to a minimum, at $r \approx 13.5$, whereas the cations go from its lower value, at $r = 5.5a$ to their bulk value at $r \approx 7.25$, and then to a maximum at $r \approx 8.625$, and then again to its bulk value, at $r \approx 12.25a$. From its maximum value $F_{MM}^s(r)$ decreases down to zero, for $r \approx 14.145$. Notice that, although the points of zero entropic and electric force are very close to each other, they do not coincide. The net force, i.e., the mean force, in this region is repulsive, implying that *the repulsive entropic force overcomes the attractive electric force*. We already pointed out that a point of zero force occurs at $r \approx 13.59a$.

The next maximum of the electrical force and minimum of the entropic force coincide at $r \approx 16.25a$. From the observation of RDFs of the macroions, anions and cations (see Fig. 2), between $r \approx 13.59a$ and $r = 26.22a$, the positive electrical force is due to the positive charge of the first layer of macroions, while the entropic attraction seems to come from the pressure of the next layer of cations–anions–macroions. The first minimum of the effective force is at $r = 15a$, and does not coincide with the nearby minimum of the entropic force, while its second maximum, at $r \approx 23.75a$, coincides with the maximum entropic force component. This structure and correlation of the RDFs, Figure 2, with the forces presented in Figure 3, are oscillatory $\forall r$. The $\lim_{r \to \infty} F_{Mi}^j(r) \to 0$, $\forall j$.

In between the subsequent layers of macroions, after the location of the second layer of macroions at $r \approx 26.22a$, a similar mechanism seems to occur, i.e., in Figure 2 we see first an adsorption of anions, above their bulk value, followed by an adsorption of cations, which together with the charge of the first layer of macroions seems to be related to the repulsive, and then attractive force of the electrical component, as a function r. Whereas the entropic force goes first from attractive, and then repulsive. So, why the electrical force is attractive?

To try to understand the role of the macroions charge, and volume fraction, on the total mean force, in Figure 4 we show this force for three different charge densities on the macroions, $\sigma_M = 0.05, 0.15$ and $0.30\,\mathrm{C/m}^2$, which correspond to $Z_M \approx 18, 53$ and 103, respectively. We keep the volume fraction constant, with $\phi = 0.12$. The forces are oscillatory. The higher the macroions' charge, the more intense the force (notice the different scales used in the figure). The higher the charge the closer and intense is the first minima of the force among the like-charged macroions, i.e., the stronger the attraction among like-charged particles. We have performed calculations of the total mean force, for a fixed macroions charge, and three different volume fractions: $\phi = 0.06, 0.12$ and 0.24 (not shown). We find that the higher the volume fraction, the closer the macroions, and stronger, and closer the attractive minima of the total mean force. This is to be expected, since higher volume fraction implies less
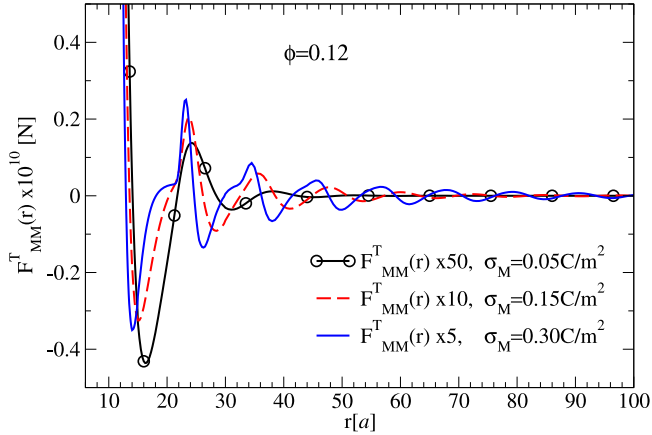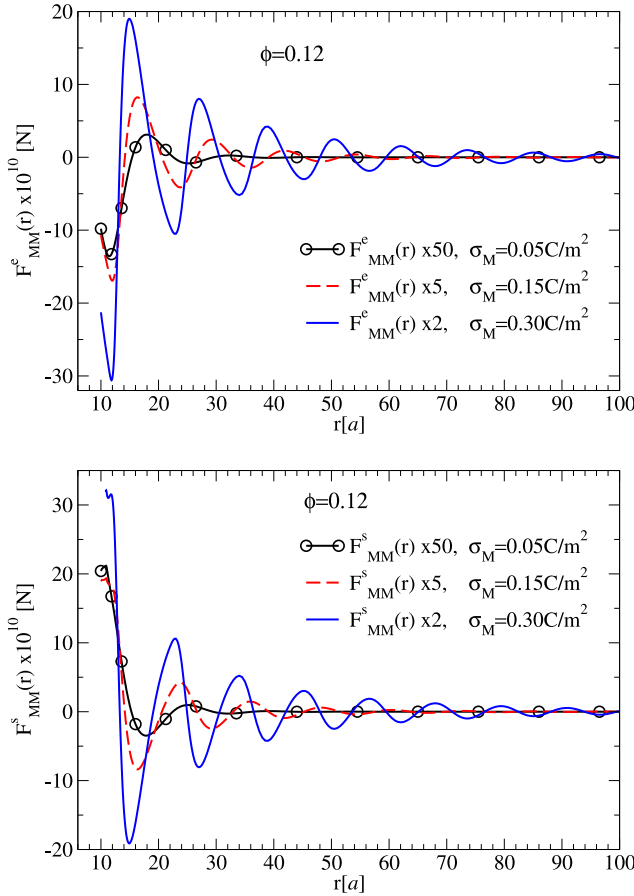
Fig. 4. Mean force among like-charged macroions, for different macroions' surface charge densities, corresponding, from lower to higher charge densities, to $Z_M \approx 18, 53$, and 106, respectively. Notice the scaling factors. r is referred to the center of the reference macroion. $\rho_{\text{salt}} = 0.1$M, $a_M = 10a$.

available volume, and stronger the entropic component of the force. However, it is a bit puzzling why higher charge implies stronger attraction among the macroions. The explanation we think is due to a combination of two effects: a higher adsorption of anions in-between layers of macroions, and that the charge repulsion among like-charged macroions also increases the excluded volume of the system, then increasing the entropic attractive force. This like-charge excluded volume depends on the amount of charge on the macroparticles and, clearly, of the system's temperature [65]. The shoulder observed around $r = 20a$, in the $\sigma_M = 0.30\,\text{C/m}^2$ curve, results from the higher gathering of the macroions, i.e., the higher the macroions charge, the closer they become (see Tab. 1).

As discussed above, beyond the fact that equations (1) and (9) are non-linear integral equations, the mean electrostatic potential, $\psi_{ij}(r)$, and mean potential of the short-range force, $\omega_{ij}^{sr}(r)$, are entangled, and, thus, also are entangled the electric, $F_{MM}^e(r)$, and entropic, $F_{MM}^s(r)$, components of the total force, $F_{MM}^T(r)$. We have performed calculation for a zero charge macroparticles, at, say, $\phi = 0.12$, and find that the entropic force (not shown), which in these conditions is equal to the total mean force, is much more less intense and of much shorter range (see Tab. 1). Therefore, we may conclude that higher macroions charge increases the gathering of the macroion, due to an important adsorption of anions around the macroions, which produces an inversion of the induced charge, $\sigma_M(r)$, i.e., the electric field, $E_M(r)$, but also due to an increase of the macroion–macroion electrostatic repulsion, which in turn increases the entropic attraction, i.e., for finite macroions' volume fractions, excluded-volume interactions are accentuated, and like-charged repulsion contributes to an even lower available volume.

In Table 1, we display the locations of the first six layers of macroions, as a function of the distance r/a to the central macroion, for different macroions charge. We see that as the charge increases, from $\sigma_M(r) = 0.050\,\text{C/m}^2$ to $\sigma_M(r) = 0.300\,\text{C/m}^2$, the macroion layers compact around the central macroion. For $\sigma_M(r) = 0.000\,\text{C/m}^2$, only the entropic force is present, and the first layer of macroions is in contact with the central macroion ($g_{MM}(r = 10a) = 1.5636$). For $\sigma_M(r) = 0.005\,\text{C/m}^2$, the first layer of macroions is still in contact with the central macroion, but with a bit less probability ($g_{MM}(r = 10a) = 1.5634$), and the subsequent layers spread a little bit

Fig. 5. Electrical, $F^e_{MM}(r)$, and entropic, $F^s_{MM}(r)$, components of the mean force among like-charged macroions, for different macroions' surface charge densities. r is referred to the center of the reference macroion. Notice the scaling factors. $\rho_{\text{salt}} = 0.1$M, $a_M = 10a$.

more. For $\sigma_M(r) = 0.025\,\text{C/m}^2$, the first layer of ions is repelled away from the central macroion, and the subsequent layers of macroions spread further away. Also notice that the macroions charge increases the range of the correlation. For the higher charges displayed in Table 1, the number of detected macroions layers go as far as $r \approx 600a$. In short, for uncharged or very little charged macroions the macroion–macroion attraction is due to the entropic force, resultant of considering the macroions volume. Higher volume fractions increases the macroions attraction. At still some very low macroions charge, i.e., $\sigma = 0.025\,\text{C/m}^2$, the first layer of macroions around the central particle is repelled away, as a result of the electrical repulsion. However, for low to high macroions charge, higher charge produces stronger macroions attraction.

In Figure 5, the electric and entropic components of the total force are presented, for the same three different macroions charge, and at a fixed volume fraction, $\phi = 0.12$, as in Figure 4, showing that in both cases their minima are all more intense, and closer to the reference macroion, for higher macroions' charge density. Being the nature of the electrical force among like-charged particles repulsive, a large attractive increase in the intensity, is probably due to the very high adsorption of anions to the positive macroions (see Fig. 2). This attraction is enhanced by the also strong attractive contribution of the entropic force, as a result of the pressure of the external layers of

the fluid, to the inner layers of ions. Additionally, one should keep in mind that both, the electric and entropic components of the mean force are entangled and, hence, a simple separation of the two contributions is not possible, since are not independent.

The shoulder seen in Figure 4 is the result of a very large increase in the first maxima of the entropic force components. The higher the charge the longer the macroion–macroion force correlation. This is also true for higher volume fractions and/or larger macroions size. The behavior of the electric force, as the macroions charge increases show its impact in the decrease of the accessible volume. Both the electric and force components increase their intensity and correlation, with increasing macroions charge.

3.2 Long-range attractive and repulsive forces: comparison with experimental results

In experimental studies of polymer latex suspensions, the range of a long-range attraction among macroions, at finite concentration, is often reported in terms of the macroion–macroion distance of closest approach, r_{ca}, which we define here as the location of the first layer of macroions, around the central macroion, or the first minimum of the macroion–macroion potential of mean force, or the first point of zero total force in Figures 3–5. We have calculated the macroion–macroion RDF for four different macroions diameters ($a_M = 10a, 20a, 30a$ and $40a$), at fixed $\phi = 0.12$, $\sigma_M = 5.355 \times 10^{-2}$ C/m^2, $\rho_{\text{salt}} = 0.1M$ (not shown). Their corresponding distances of macroion–macroion closest approach are $r_{ca} = 1.41a_M, 1.33a_M, 1.27a_M$ and $1.24a_M$, respectively. As a general behavior, larger macroions size implies higher concentration, of the first layer of the attracted macroions, and shorter values of r_{ca}, although of course, in units of a, r_{ca} increases with increasing a_M.

A *direct* comparison of our theory with experimental for very large macroions, such as those reported for polystyrene latex particles [8,22,66,67], where the macroion sizes are in the range of 3000 Å–8000 Å is beyond the scope of this paper. Fortunately, however, there are some experimental data for smaller polystyrene latex particles, such as those reported in Ottewill [7]. In Figure 6, we present a comparison of the RDF for two different sets of parameters: (a) $\phi = 0.01$, $\sigma_M = 1.25 \times 10^{-3}$ C/m^2, and (b) $\phi = 0.13$, $\sigma_M = 3.90 \times 10^{-3}$ C/m^2. In both cases $a_M = 74a = 314.5$ Å, and $\rho_{\text{salt}} = 1.0 \times 10^{-4}$ M. The experimental data parameters are (a) $\phi = 0.01$ and (b) $\phi = 0.13$. In both cases $a_{M\text{exp}} \approx 310$ Å $\approx 73a$ and $\rho_{\text{salt}} = 1.0 \times 10^{-4}$ M. He did not report measured macroions' surface charge densities, but fitted macroions' surface mean electrostatic potentials, of the order 50 mV. In our calculations, the macroions's surface potential are both of the order of 17 mV. Hence, although we cannot make a direct quantitative comparison with these experimental results, our calculations parameters closely resemble those reported by Ottewill. The qualitative agreement of our Figure 6 with the Figure 4 of Ottewill's paper is very good. Moreover, he reported values of r_{ca} of 1000 Å $= 3.22a_{M\text{exp}}$ and 500 Å $= 1.61a_{M\text{exp}}$, obtained from his RDFs for his $\phi = 0.01$ and $\phi = 0.13$, respectively. In our case, we find r_{ca} of 1145.8 Å $= 3.64a_M$ and 483 Å $= 1.54a_M$, for $\phi = 0.01$ and $\phi = 0.13$, respectively.

We did perform calculations for macroions as large as $340a_M$, for different salt concentrations, macroions's charge and volume fractions (not shown), and as a general trend we find that the r_{ca} parameter scales with the macroion's size, and that increasing a_M and/or ϕ and/or σ_M and/or ρ_{salt}, decreases r_{ca}. Nevertheless, different combinations of these parameters can produce very large values of r_{ca}, as we have shown. Clearly, the larger the macroion's size, the larger the location of the first attractive minimum in the macroion–macroion potential of mean force. Experimental results for macroions of 6000 Å of diameter, and surfaces charges of
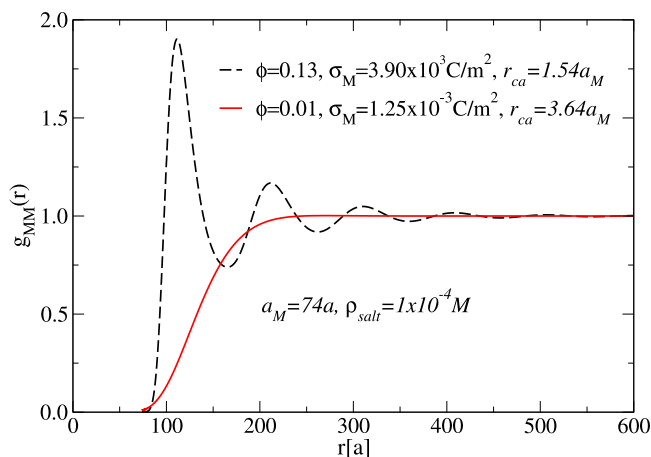
Fig. 6. Radial distribution function, around the central macroion, for two different volume fractions and surface charge densities. r is referred to the center of the corresponding reference macroion.

$\sigma = 2.7 \times 10^{-2}\,\mathrm{C/m^2}$, and $\sigma = 3.0 \times 10^{-3}\,\mathrm{C/m^2}$, reported by Tata et al. [22], have values of $r_{ca} = 2.42a_{M\exp}$ and $r_{ca} = 2.47a_{M\exp}$, respectively. Those reported by Ise et al. [8] show similar results for their 4190 Å diameter, and $\sigma = 7.25 \times 10^{-2}\,\mathrm{C/m^2}$, polystyrene particles, i.e., for $\phi = 0.0075$ and $\phi = 0.112$, they find $r_{ca} = 3a_{M\exp}$ and $r_{M\exp} = 1.695a_{M\exp}$.

While our r_{ca} results confirm the existence of a long-range macroions attraction, and have a good qualitative agreement with some experimental data, we wish to emphasize the relevance of the truly very long range of the oscillatory macroion–macroion RDF and force, which may have relevant consequences in several soft condensed matter and biological systems [56,57].

4 Discussion

The objective of this research was to explore the nature of the mean forces present in a highly charged macroions solution, at a finite volume fraction, ϕ, with a well-established liquid theory. The experiments of Ise et al., where an order–disorder coexistence regions are reported [8–11], imply the existence of long-range attractive forces among like-charged macroions. However, these long-range forces cannot be explained in terms of conventional direct interaction potentials, which are of short range [12]. Semi-phenomenological long-range potentials have been proposed in the past [13–15]. Ise et al. [13,23,24] have proposed that this attraction is due to "*an intermacroion attraction through the intermediary of counterions balanced by intermacroion repulsion*". While in this article we did not pretend to find a coexistence curve, and do not take a strong position on the details of the experimental results, we solved the well-established HNC/MSA liquid theory, applied to a CPM, obtained the macroion–macroion, macroion–anion and macroion–cation RDFs, and calculated the electrical field and the mean forces among the like-charged macroions. Our study shows that higher macroions charge increases the gathering of the macroions, due to an important adsorption of anions around the macroions, which produces an inversion of the induced charge, $\sigma_M(r)$, i.e., the electric field, $E_M(r)$, but also due to an increase of the macroion–macroion electrostatic repulsion, which in turn increases the entropic attraction, i.e., for finite macroions' volume fractions, excluded-volume

interactions are accentuated, and like-charged repulsion contributes to an even lower available volume.

Our findings are in agreement with two aspects of the experimental results of Tata et al. [11,20–22]: like charged particles get closer among them with higher electrical charge, and there is a very long-range attractive–repulsive correlation. *Our calculations are with no assumption of a long-range attractive potential or confining wall, and the system is certainly at equilibrium, since the integral equations are basically a chemical potential balance equation.* While our results seem to indicate that the high adsorption of anions in between two neighboring layers of macroions explain in part the attraction among the like-charged macroions, as proposed by Ise et al. [13,23,24], the fact that the electrical and entropic forces are entangled, through the non-linearity of the RDFs equations of the CPM (Eqs. (1) and (9)), imply that the electrical component also contributes to an excluded volume effect, and, hence, is also in part responsible for the attractive force among like-charged macroions.

In particular, our RDF calculations, for macroions' parameters corresponding to those of the experimental RDFs reported by Ottewill [7], show a very good qualitative agreement. In particular, in relation to the range of the macroions long-range attractive interaction.

As a general result we find that the range of the attractive-repulsive forces, among the macroions, scales with the macroion's size, and that increasing the macroion size and/or their volume fraction and/or charge and/or the salt concentration, increases the macroions attraction. Nevertheless, different combinations of these parameters can produce very long-range macroion–macroion attractions, as we have shown. Clearly, the larger the macroion's size, the larger the range of the first attractive minimum in the macroion–macroion potential of mean force.

As a main conclusion we stress that our theoretical calculations are based on a well-established integral equation theory, shown in the past to be in agreement with computer simulation data, we have not used any adjustable parameter, and have proved the existence of very long-range attractive–repulsive forces, in macroions dispersions at finite volume fraction, and that are in agreement with experimental results.

References

1. P. Pieransky, Contemp. Phys. **24**, 25 (1983)
2. E.A. Kamenetzky, L.G. Magliocco, H.P. Panzer, Science **263**, 207 (1994)
3. D.F. Evans, H. Wennerström, *The Colloidal Domain: Where Physics, Chemistry, Biology, and Technology Meet*, 2nd edn. (Wiley-VCH, New York, 1999)
4. J. Vatamanu, D. Bedrov, J. Phys. Chem. Lett. **6**, 3594 (2015)
5. N.A. Clark, A.J. Hurd, B.J. Ackerson, Nature **281**, 57 (1979)
6. N. Ise, T. Okubo, Acc. Chem. Res. **13**, 303 (1980)
7. R.H. Ottewill, Langmuir **5**, 4 (1989)
8. N. Ise, T. Okubo, M. Sugimura, K. Ito, H.J. Nolte, J. Chem. Phys. **78**, 536 (1983)
9. H. Matsuoka, H. Nakamura, H. Okumura, T. Ono, I.S. Sogami, J.Y. Ueno, H. Yoshida, T. Yoshiyamal, Langmuir **9**, 394 (1993)
10. K. Ito, H. Yoshida, N. Ise, Science **263**, 66 (1994)
11. B.V.R. Tata, E. Yamahara, P.V. Rajamani, N. Ise, Phys. Rev. Lett. **78**, 2660 (1997)
12. Y. Min, M. Akbulut, K. Kristiansen, Y. Golan, J. Israelachvili, Nat. Mater. **7**, 527 (2008)
13. I. Sogami, N. Ise, J. Chem. Phys. **81**, 6320 (1984)
14. N. Ise, Ber. Bunsenges. Phys. Chem. **10**, 841 (1996)

15. I.S. Sogami, Chem. Lett. **41**, 1331 (2012)
16. M. Evers, N. Garbow, D. Hessinger, T. Palberg, Phys. Rev. Lett. **72**, 786 (1994)
17. J.C. Crocker, D.G. Grier, Phys. Rev. Lett. **77**, 1897 (1996)
18. R. van Roij, J.P. Hansen, Phys. Rev. Lett. **79**, 3082 (1997)
19. K.S. Schmitz, Phys. Rev. E **65**, 061402(1) (2002)
20. B.V.R. Tata, A.K. Arora, Phys. Rev. Lett. **72**, 787 (1994)
21. B.V.R. Tata, N. Ise, Phys. Rev. E **61**, 983 (2000)
22. B.V.R. Tata, P.S. Mohanty, M.C. Valsakumara, Solid State Commun. **147**, 360 (2008)
23. N. Ise, T. Okubo, J. Phys. Chem. **70**, 1930 (1966)
24. N. Ise, Phys. Chem. Chem. Phys. **12**, 10279 (2010)
25. H. Manzanilla-Granados, M. Lozada-Cassou, J. Phys. Chem. B **117**, 11812 (2013)
26. E.J.W. Verwey, J.T.G. Overbeek, *Theory of the Stability of Lyophobic Colloids* (Dover, New York, 1948)
27. F.H. Stillinger, J.G. Kirkwood, J. Chem. Phys. **33**, 1282 (1960)
28. M. Medina-Noyola, D. McQuarrie, J. Chem. Phys. **73**, 6279 (1980)
29. K.S. Schmitz, *Macroions in Solution and Colloidal Suspensions* (VCH Publishers, New York, 1993)
30. R. Kjellander, S. Marčelja, Chem. Phys. Lett. **127**, 402 (1986)
31. A. Diehl, M.N. Tamashiro, M.C. Barbosa, Y. Levin, Physica A **274**, 433 (1999)
32. L. Belloni, J. Phys.: Condens. Matter **12**, R549 (2000)
33. T. Colla, M. Girotto, A.P. dos Santos, Y. Levin, J. Chem. Phys. **145**, 094704 (2016)
34. L. Belloni, Colloids Surf. A **140**, 227 (1998)
35. L. Bocquet, E. Trizac, M. Aubouy, J. Chem. Phys. **117**, 8138 (2002)
36. N. Ise, T. Konishi, B.V.R. Tata, Langmuir **15**, 4176 (1999)
37. L.E. Sánchez-Díaz, G.A. Mendez-Maldonado, M. González-Melchor, H. Ruiz-Estrada, M. Medina-Noyola, J. Chem. Phys. **135**, 014504 (2011)
38. P. Linse, V. Lobaskin, Phys. Rev. Lett. **83**, 4208 (1999)
39. P. Linse, V. Lobaskin, J. Chem. Phys. **112**, 3917 (2000)
40. V. Lobaskin, K. Qamhieh, J. Phys. Chem. B **107**, 8022 (2003)
41. J.G. Kirkwood, J.C. Poirier, J. Phys. Chem. **58**, 591 (1954)
42. D.A. McQuarrie, *Statistical Mechanics* (Harper and Row, New York, 1976)
43. M. Lozada-Cassou, in *Fundamentals of Inhomogeneous Fluds*, edited by D. Henderson (Marcel Dekker, New York, 1992), Chap. 8
44. P. Attard, in *Advances in Chemical Physics*, edited by I. Prigogine, S.A. Rice (John Wiley and Sons, Inc., New York, 1996), Vol. XCII
45. S.L. Carnie, D.Y.C. Chan, D.J. Mitchell, B.W. Ninham, J. Chem. Phys. **74**, 1472 (1981)
46. H.M. Manzanilla-Granados, F. Jiménez-Ángeles, M. Lozada-Cassou, Colloids Surf. A **376**, 59 (2011)
47. H.M. Manzanilla-Granados, F. Jiménez-Ángeles, M. Lozada-Cassou, J. Phys. Chem. B **115**, 12094 (2011)
48. H. Greberg, R. Kjellander, Chem. Phys. Lett. **200**, 76 (1992)
49. D.M. Zuckerman, M.E. Fisher, S. Bekiranov, Phys. Rev. E **64**, 011206 (2001)
50. G. Odriozola, M. Lozada-Cassou, Fortschr. Phys. **65**, 1600072 (2017)
51. H.L. Friedman, *A Course in Statistical Mechanics* (Prentice-Hall, Inc., NJ, 1985)
52. K. Hiroike, Mol. Phys. **33**, 1195 (1977)
53. J.E. Sánchez, M. Lozada-Cassou, Chem. Phys. Lett. **190**, 202 (1992)
54. L. Yeomans, S.E. Feller, E. Sánchez, M. Lozada-Cassou, J. Chem. Phys. **98**, 1436 (1993)
55. W.F. Lawless, J. Math. Psychol. **78**, 51 (2017)
56. J.A. González-Calderón, M. Chávez-Páez, E. González-Tovar, M. Lozada-Cassou, arXiv:1712.00467v1 [cond-mat.soft] (2017)
57. J.A. González-Calderón, M. Chávez-Páez, E. González-Tovar, M. Lozada-Cassou, J. Phys. Chem. B **122**, 7002 (2018)
58. D. Henderson, M. Lozada-Cassou, L. Blum, J. Chem. Phys. **79**, 3055 (1983)
59. M. Lozada-Cassou, R. Saavedra-Barrera, D. Henderson, J. Chem. Phys. **77**, 5150 (1982)
60. E. Gonzales-Tovar, M. Lozada-Cassou, D. Henderson, J. Chem. Phys. **83**, 361 (1985)
61. E. González-Tovar, M. Lozada-Cassou, J. Chem. Phys. **93**, 3761 (1989)

62. M. Lozada-Cassou, E. Díaz-Herrera, J. Chem. Phys. **92**, 1194 (1990)
63. F. Jiménez-Ángeles, M. Lozada-Cassou, J. Phys. Chem. B **108**, 7286 (2004)
64. F. Jiménez-Ángeles, G. Odriozola, M. Lozada-Cassou, J. Phys.: Condens. Matter **21**, 424107 (2009)
65. C. Deutsch, Y. Furutani, M. Gomber, Phys. Rep. **69**, 85 (1981)
66. P.A. Rundquist, S. Jagannathan, R. Kesavamoorthy, C. Brnardic, S. Xu, S.A. Asher, J. Chem. Phys. **94**, 711 (1991)
67. N. Ise, M.V. Smalley, Phys. Rev. B **50**, 16722 (1994)